forum acusticum 2026
8-12 September · Graz, Austria

DATA-DRIVEN DYNAMICAL ENERGY ANALYSIS FOR MODELLING HIGH-FREQUENCY NOISE AND VIBRATION

David J. Chappell[1], Lama Hamadeh[2]

[1] *Department of Physical Sciences, Nottingham Trent University, UK*
[2] *Department of Mechanical Engineering, University College London, UK*

Abstract

Predicting high-frequency noise and vibration in complex structures is a challenging task where standard numerical methods for wave-based models struggle with the rapid oscillations involved, leading to prohibitive computational costs. Dynamical Energy Analysis (DEA) offers a robust solution by using a transfer operator to track ray densities in phase-space, providing a ray-based methodology that is not restricted by the reflection order. This research introduces a data-driven version of DEA, based on an Extended Dynamic Mode Decomposition (EDMD) construction of the DEA transfer operator. The shift of focus from ray geometry to ray data facilitates a subdivision of the phase-space data into clusters where the pre-image of the ray flow map is locally smooth. The accuracy may then be further enhanced by using Legendre polynomial basis expansions within these clusters and/or the further sub-division of the phase-space. Numerical experiments focussed on simple benchmark tests will be presented to demonstrate the accuracy, effectiveness and potential of the proposed methodology for future extension to built-up structures and industry inspired applications.

Keywords: *high-frequency waves, extended dynamic mode decomposition, data-driven methods, dynamical energy analysis*

1. Introduction

Determining high-frequency mechanical wave fields in complex structures is a challenging problem in applied mathematics, with numerous important applications [1]–[3]. High-frequency noise and vibration are typically modelled by partial differential equations with highly oscillatory solutions, which when combined with the complex geometries encountered in real industrial applications can lead to very large and computationally costly numerical schemes [4]–[6]. As a consequence, ray-based approaches are often employed to avoid the high computational costs associated with the direct numerical simulation of the oscillatory wave problem [1], [3], [7]. One such method is Dynamical Energy Analysis (DEA) [5], which models wave energy transport through complex structures using a linear transfer operator known as the Frobenius–Perron operator. This operator describes the evolution of ray-density distributions in phase space, providing an efficient framework for approximating high-frequency wave energy flow [8].

Despite its advantages, DEA faces a significant limitation: its numerical convergence is typically restricted to first-order for geometries containing corners in two dimensions or edges in three dimensions [9], while faster convergence can be obtained in smooth geometries [10]. The root cause of this limitation relates to jump discontinuities in the underlying ray map embedded within the transfer operator. At these corners and edges, ray trajectories undergo abrupt changes of reflected direction. As a result, standard numerical approximation methods struggle to resolve these discontinuities accurately, which limits convergence. This work aims to develop the first data driven implementation of DEA that will treat discontinuities in phase-space using data partitioning algorithms, and approximate the Frobenius-Perron transfer operator using Extended Dynamic Mode Decomposition (EDMD) [11], [12].

2. Propagating phase-space densities via transfer operators

A framework for propagating densities along ray trajectories within a domain Ω can be formulated using the Frobenius–Perron (FP) transfer operator. Specifically, in DEA we apply the FP operator to transport phase-space densities between instances when the ray trajectory intersects the boundary of Ω, which we

***Corresponding author**: david.chappell@ntu.ac.uk.*

denote Γ [5]. In this section, the FP operator is introduced along with its approximation via the EDMD algorithm. We then describe the formulation of an initial density associated with a noise or vibration source. Finally, the interior density is constructed, providing a solution for the total acoustic or vibrational energy density at specified positions within Ω.

2.1. Frobenius–Perron transfer operator

Consider the dynamical system $(\mathcal{X}, \Phi)$, with $\mathcal{X} = \Gamma \times (-\eta, \eta)$ the phase space corresponding to the boundary Γ of a domain $\Omega \subset \mathbb{R}^2$, together with the momentum or slowness coordinate prescribing the tangential (to Γ) component of the propagation direction scaled by the inverse of the wave speed $\eta = 1/c$. The map $\Phi : \mathcal{X} \to \mathcal{X}$ is the ray-tracing boundary flow map taking a point (parametrised by arclength) $s \in \Gamma$ along the direction prescribed by $p \in (-\eta, \eta)$ to the position s' obtained when the the trajectory next intersects Γ, along with the direction p' given by a specular reflection of the ray at s'. We may write $p = \eta \sin\theta$, where $\theta \in (-\pi/2, \pi/2)$ denotes the angle between the interior normal vector and the outgoing ray at the point s. If $\boldsymbol{x} = (s, p) \in \mathcal{X}$, then the evolution of its phase-space densities under the underlying ray dynamics can be described using the FP transfer operator, $\mathcal{P}$. For a density f, the transfer operator $\mathcal{P}$ is defined as

$$\mathcal{P}f(\boldsymbol{y}) = \int_{\mathcal{X}} f(\boldsymbol{x})\delta(\boldsymbol{y} - \Phi(\boldsymbol{x}))\mathrm{d}\boldsymbol{x}. \tag{1}$$

This operator governs the transport of densities under a dynamical system by mapping f through a given propagation step. In this work, it provides a framework for tracking how acoustic or vibrational energy densities evolve along ray trajectories in phase space. The Frobenius–Perron operator is linear and it acts on an infinite-dimensional function space. Despite the nonlinear nature of the underlying dynamical system, the operator describes it in a linear framework. This linearity is a key advantage, as it enables the reformulation of nonlinear transport problems into linear operator equations acting on phase-space distributions. Due to its infinite-dimensional nature, practical computation of the Frobenius–Perron operator requires numerical approximation. In this work, the FP operator is approximated via the EDMD algorithm, which allows for an efficient data-driven representation of its action on a chosen basis of phase-space functions.

2.2. Extended Dynamic Mode Decomposition

In order to approximate FP operator $\mathcal{P}$ using EDMD, we first partition the phase-space into N_{par} non-overlapping partitions E_i and introduce a decomposition of our phase-space density f into its values within these partitions as follows

$$f(\boldsymbol{x}) = \sum_{i=1}^{N_{\mathrm{par}}} \psi_i(\boldsymbol{x}), \tag{2}$$

where $\psi_i(\boldsymbol{x})$ defines a basis expansion associated with partition E_i and $\psi_i(\boldsymbol{x}) = 0$ for $\boldsymbol{x} \notin E_i$. Scaled Legendre polynomials of total degree P are employed for the basis functions in both the spatial coordinate s and the directional coordinate p. The choice of Legendre polynomials is motivated by their orthogonality properties over bounded intervals, which can be beneficial for conditioning and stability. To implement these Legendre polynomial basis functions, we first enclose each partition $E_i \subset \mathcal{X}$ in the smallest possible Cartesian bounding box $B_{E_i} = \left(s_c - \frac{h_s}{2}, s_c + \frac{h_s}{2}\right) \times \left(p_c - \frac{h_p}{2}, p_c + \frac{h_p}{2}\right)$ with side-lengths h_s and h_p, and centroid (s_c, p_c). We define the affine map as

$$(\tilde{s}, \tilde{p}) = \tilde{\boldsymbol{x}} = \left(\frac{2\,(s - s_c)}{h_s}, \frac{2\,(p - p_c)}{h_p}\right), \tag{3}$$

which carries B_{E_i} on to the reference box $\tilde{B}_{E_i} = (-1, 1)^2$. Accordingly, the basis expansion is defined locally on each partition as $\psi_i(\boldsymbol{x}) =$

$$\begin{cases} \sum_{j=0}^{P} \sum_{k=0}^{P-j} f^i_{j,k}\, L^i_j(\tilde{s}) L^i_k(\tilde{p}) & \text{if } (s,p) \in E_i, \\ 0 & \text{otherwise,} \end{cases} \tag{4}$$

where $f^i_{j,k}$ are the basis expansion coefficients in E_i, and L^i_j and L^i_k denote the scaled Legendre polynomials of degree j and k in the normalised coordinates $\tilde{s}$, and $\tilde{p}$, respectively. The scaling of the Legendre polynomials is implemented by introducing a pre-factor of $\sqrt{(2j+1)/h_s}$ for $L^i_j(\tilde{s})$ and $\sqrt{(2k+1)/h_p}$ for $L^i_k(\tilde{p})$.

In EDMD, the approximated FP operator $\mathbf{P}$ is constructed from a set of M trajectory data points $\boldsymbol{x}_m = (s_m, p_m)$ for $m = 1, \ldots, M$. Given this data, together with the corresponding mapped data $\Phi(\boldsymbol{x}_m)$ for $m = 1, \ldots, M$, then the EDMD approximation of the FP operator is defined as

$$\mathbf{P} = \mathbf{H}^{-1}\mathbf{G}. \tag{5}$$

Here, $\mathbf{H}$ is a block-matrix comprising $N_{\mathrm{par}} \times N_{\mathrm{par}}$ square blocks of length $(P+1)(P+2)/2$. For $i, i' = 1, 2, \ldots N_{\mathrm{par}}$, these blocks $\mathbf{H}_{i,i'}$ contain entries of the form

$$\frac{1}{M} \sum_{m=1}^{M} L^i_j(\tilde{s}_m) L^i_k(\tilde{p}_m) L^{i'}_{j'}(\tilde{s}_m) L^{i'}_{k'}(\tilde{p}_m).$$

The matrix $\mathbf{H}$ is primarily associated with the normalisation of the basis. The indexing for each Legendre polynomial pair (j, k) or (j', k') within the matrix block entries runs with the same ordering as in the double sum in (4), increasing with row number for the pair with superscript i, and with column number for the pair with superscript i'.

Likewise, the matrix $\mathbf{G}$ has the same $N_{\mathrm{par}} \times N_{\mathrm{par}}$ block structure with square blocks of length $(P+1)(P+2)/2$.

For $i, i' = 1, 2, \ldots N_{\text{par}}$, these blocks, $\mathbf{G}_{i,i'}$ have entries

$$\frac{1}{M}\sum_{m=1}^{M} e^{-\mu R} L_j^i(\tilde{\Phi}_s(\boldsymbol{x}_m)) L_k^i(\tilde{\Phi}_p(\boldsymbol{x}_m)) L_{j'}^{i'}(\tilde{s}_m) L_{k'}^{i'}(\tilde{p}_m).$$

The matrix $\mathbf{G}$ describes the mapping of a boundary density between sending and receiving partitions under the ray dynamics. As with the blocks $\mathbf{H}_{i,i'}$, the index pair (j, k) increases with the row number taking the same values as prescribed by the double sum in (4), and likewise (j', k') for the columns. The rows of $\mathbf{G}$ correspond to receiving ray partition indices, while the columns correspond to sending ray partition indices. The exponential pre-factor is included to account for dissipation arising from, for example, structural damping. Here, μ is the (locally constant) attenuation coefficient and R denotes the Euclidean length of the ray from s to $\Phi_s(\boldsymbol{x}_m)$. Note that we have decomposed the flow map Φ into its separate arclength position and tangential slowness coordinates written as $\Phi(\boldsymbol{x}_m) = (\Phi_s(\boldsymbol{x}_m), \Phi_p(\boldsymbol{x}_m))$. The tildes are used to represent normalisation via the map (3) as before.

Once we have our finite dimensional approximation $\mathbf{P}$ of the FP operator, then we may use it to propagate an initial phase-space density f_0 through arbitrarily many boundary reflections to obtain a stationary density f. We can obtain the basis expansion coefficients for f in a vector $\boldsymbol{f} = [f_{0,0}^1 f_{0,1}^1 \cdots f_{P,0}^1 f_{0,0}^2 \cdots f_{P,0}^{N_{\text{par}}}]^T$ by taking a sum over multiple iterations of the approximated FP operator via

$$\boldsymbol{f} = \sum_{n=0}^{\infty} \mathbf{P}^n \boldsymbol{f}_0. \tag{6}$$

Here, $\boldsymbol{f}_0$ is the vector of basis coefficients obtained by Galerkin projecting the initial density f_0 onto the same basis. Using a Neumann series argument and assuming the spectrum of $\mathbf{P}$ is contained within the unit circle (this will be true for $\mu > 0$), then the evaluation of $\boldsymbol{f}$ reduces to solving the linear system

$$(\mathbf{I} - \mathbf{P})\,\boldsymbol{f} = \boldsymbol{f}_0, \tag{7}$$

where $\mathbf{I}$ is the identity matrix. Equation (7) provides a complete description of the steady-state boundary phase-space density resulting from repeated ray propagation and boundary interactions.

2.3. Source representation and initial densities

We consider a boundary source located along a subset of the boundary $\Gamma_0 \subset \Gamma$. We take the source to be spatially constant along Γ_0 and assume that it is concentrated in a single prescribed direction travelling into Ω. The source is therefore localised to a single momentum coordinate $p = p_0$. The initial density of the boundary source is therefore written as:

$$f_0(s, p) = \chi_{\Gamma_0}(s)\delta(p - p_0), \tag{8}$$

where $\chi_{\Gamma_0}(s)$ denotes an indicator function with support along Γ_0 and $\delta(p - p_0)$ is a Dirac delta concentrated at the prescribed tangential momentum p_0.

2.4. Interior density reconstruction

The interior density describes the distribution obtained after propagating the stationary density f into Ω. The interior density at a point $\boldsymbol{r}$ within our domain is obtained by integrating the contribution from f arriving at $\boldsymbol{r}$ from Γ. This can be naturally expressed as an integral over the global direction $\Theta \in [0, 2\pi)$ arriving at $\boldsymbol{r} \in \Omega$ which, after a change of variables, is equivalently written as a boundary integral around Γ. The resulting expression is given by [13]:

$$\begin{aligned} f_\Omega(\boldsymbol{r}) &= \int_0^{2\pi} e^{-\mu d(\boldsymbol{r},s)} f(s,p)\mathrm{d}\Theta \\ &= \eta^2 \int_\Gamma e^{-\mu d(\boldsymbol{r},s)} f(s,p) \frac{\cos(\phi(\boldsymbol{r},s))}{d(\boldsymbol{r},s)} \mathrm{d}s. \end{aligned} \tag{9}$$

Here, the stationary density f is evaluated on each phase-space partition using its expansion in terms of Legendre polynomial basis functions in both the spatial and directional coordinates. Specifically, it is approximated by combining (2) and (4) as:

$$f(s,p) \approx \sum_{i=1}^{N_{\text{Par}}} \sum_{j=0}^{P} \sum_{k=0}^{P-j} f_{j,k}^i L_j^i(\tilde{s}) L_k^i(\tilde{p}). \tag{10}$$

Numerically, the integral in Equation (9) is approximated using a quadrature rule applied over each partition. Note that $d(\boldsymbol{r}, s)$ is the Euclidean distance between the integration point s along Γ and the evaluation point $\boldsymbol{r}$ within the domain. The angle $\phi(\boldsymbol{r}, s) \in (-\pi/2, \pi/2)$ is formed between the interior normal to Γ at s and the ray leaving s and arriving at $\boldsymbol{r}$. Directions oriented anticlockwise with respect to Γ are positive.

3. Data-driven phase-space partitioning

The phase-space partitioning process is defined by the pre-image Φ^{-1} of mapping between sending and receiving boundary edges for each ray trajectory. Starting from the set of sending data points along the boundary of a convex polygonal domain, it is evident that rays emitted from any given edge could have arrived from all other remaining edges. The direction component θ of a ray emitted into the domain from Γ varies from $-\pi/2$ to $\pi/2$, taking the value $\theta = 0$ when travelling in the normal direction and taking positive values when its tangential component is anti-clockwise along Γ. This ray would have arrived from the other edges of Γ in an ordered sequence as θ is increased: firstly from the edge connected to the right of the current one, then the remaining opposite edges in anticlockwise order and finally the edge connected to the left of the current edge. Thus, for a ray leaving the first (labelled) edge of an N-sided convex polygon with

edges numbered in anti-clockwise order, the possible pre-image mappings are $2 \to 1$, $3 \to 1$, ..., $N \to 1$. The same ordering principle applies analogously to all edges. This grouping procedure enables the assignment of a unique index to each sending partition. Each partition represents a set of rays arriving from a specific edge and then being sent from a specified sending edge (edge 1 in the example above).

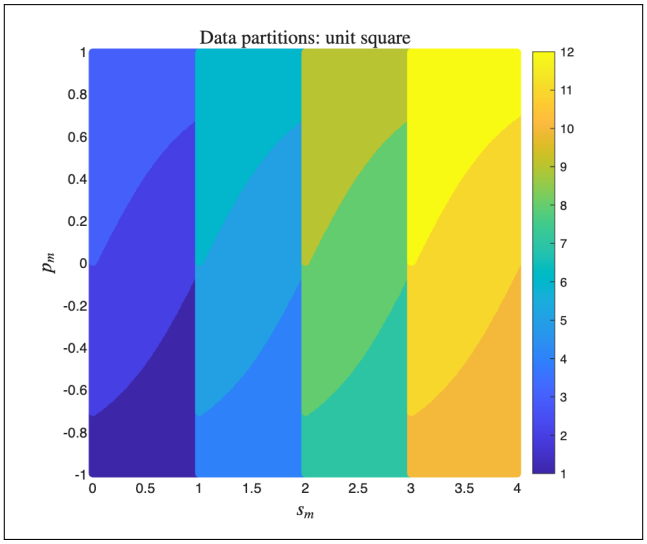

Figure 1: Data partitions for a unit square domain based on subdividing the ray trajectory data at discontinuities in the pre-image Φ^{-1} of the ray flow map. The position data values s_m, $m = 1, \ldots, M$ parametrise the boundary of the square by arclength. The momentum data values p_m, $m = 1, \ldots, M$ prescribe the tangential component of the outgoing ray vector of unit length. The plot is shown with $M = 250000$ regularly spaced data points.

Using this approach on a quadrilateral domain, for example, the minimum number of distinct sending partitions is 12 as shown for a unit square domain in Figure 1. Each sending partition is associated with a corresponding receiving partition, which is assigned a unique receiving index. This index is determined by treating the intersection point of the original ray as a new sending point and considering the pre-image once again. The boundary edge on which this point lies is first identified, followed by the determination of the angular region corresponding to its incoming direction. By following this procedure, two vectors of partition indices, one for the sending partitions and one for the receiving partitions, can be constructed. Although this minimal partitioning provides the geometric foundation of the method, further subdivision into sub-partitions in p may be required to achieve numerical convergence for highly directional source terms such as the initial density f_0 introduced in Section 2.3. To illustrate this procedure, a directional partition size parameter, Δp, is introduced to control the subdivision process. The number of directional sub-partitions is then determined from the ratio of the partition's angular range to Δp. Since the angular widths of the geometric partitions are not uniform, each primary partition may generate a different number of directional sub-partitions.

4. Numerical results

To assess the accuracy and convergence of our data-driven phase-space partitioning method, the numerical interior density given by Equation (9) is compared against an exact solution. The comparison is performed by evaluating the relative L_1 error between the numerical and exact interior density solutions over a set of N_Ω evaluation points $\boldsymbol{r}_\alpha$, $\alpha = 1, \ldots, N_\Omega$ which is given by:

$$\text{Error}_{L_1} = \frac{\sum_{\alpha=1}^{N_\Omega} \left| f_\Omega(\boldsymbol{r}_\alpha) - f_\Omega^{\text{Exact}}(\boldsymbol{r}_\alpha) \right|}{\sum_{\alpha=1}^{N_\Omega} \left| f_\Omega^{\text{Exact}}(\boldsymbol{r}_\alpha) \right|}. \tag{11}$$

We consider the boundary source (8) in a unit square domain $(0,1) \times (0,1)$ with $p_0 = 0$ and Γ_0 taken to be the left edge of the square. An exact expression for the interior density can be derived by summing the contributions from rays propagating between the left and right edges. In this case, the left boundary contributes the right-propagating attenuated rays, while the opposite boundary accounts for the left-propagating contributions. Accordingly, for a source distributed along the left edge, the exact interior density is given by:

$$f_\Omega^{\text{Exact}}(\boldsymbol{r}) = \frac{\cosh(\mu(x-1))}{\sinh(\mu)}, \tag{12}$$

where $\boldsymbol{r} = (x, y)$ denotes the interior spatial coordinate.

Table 1: The relative L_1 error and estimated order of convergence (EoC) for the interior density f_Ω with attenuation parameter $\mu = \pi/2$ and computed with $M = 250000$ data points.

Δp	Error_{L_1}	EoC
1.0	4.23e-1	-
0.5	1.12e-1	1.9
0.2	4.03e-2	1.1
0.075	5.20e-3	2.1
0.03	2.73e-3	0.7
0.02	9.59e-4	2.6
0.01	1.26e-4	2.9

Numerical simulations were performed using piecewise constant basis functions, i.e., $P = 0$ since the exact solution takes constant values along Γ, meaning $P = 0$ should be sufficient to match the exact solution. The method demonstrates excellent agreement with the exact solution. In particular, Table 1 shows that the relative L_1 error decreases to 1.26×10^{-4} for $\Delta p = 0.01$. The estimated convergence rate does not show any clear trend however, varying between 0.7 and 2.9 and behaving around second order on average, but increasing towards third order for small

enough Δp.

5. Conclusion

This work has presented a data-driven DEA approximation of high-frequency vibrational energy distributions in bounded convex polygonal domains by evaluating the Frobenius–Perron operator within an EDMD framework. By combining a phase-space partitioning method with a Legendre polynomial basis expansion, the proposed approach provides a systematic methodology for modelling the propagation of vibrational energy along ray trajectories. The numerical results demonstrate the convergence of the data-driven DEA approximation. Overall, the presented methodology offers a robust approach for the prediction of high-frequency vibrational energy distributions and provides a strong foundation for future extensions to more complex structural geometries, sources types, and vibro-acoustic industry applications.

6. Acknowledgments

We gratefully acknowledge funding from the Engineering and Physical Sciences Research Council, UK (grant number UKRI 2393).

References

[1] V. Cervený, *Seismic Ray Theory*. Cambridge, UK: Cambridge University Press, 2001, vol. 110.

[2] L. Cremer, M. Heckl, and B. Petersson, *Structure-borne sound*, 3rd ed. Berlin: Springer, 2005.

[3] H. Kuttruff, *Room Acoustics*, 6th ed. Boca Raton, United States: CRC Press, 2016.

[4] B. Engquist and O. Runborg, "Computational high frequency wave propagation", *Acta Numerica*, vol. 12, pp. 181–266, 2003.

[5] G. Tanner, "Dynamical energy analysis — determining wave energy distributions in vibro-acoustical structures in the high frequency regime", *Journal of Sound and Vibration*, vol. 320, no. 4-5, pp. 1023–1038, 2009.

[6] J. Rowbottom and D. J. Chappell, "On hybrid convolution quadrature approaches for modeling time-domain wave problems with broadband frequency content", *Int. J. Numer. Methods Eng.*, vol. 122, no. 24, pp. 7581–7608, 2021.

[7] L. Savioja and U. Svennson, "Overview of geometrical room acoustic modelling techniques", *Journal of the Acoustical Society of America*, vol. 138, no. 2, pp. 708–730, 2015.

[8] D. Chappell, J. J. Crofts, M. Richter, and G. Tanner, "A direction preserving discretization for computing phase-space densities", *SIAM J. Sci. Comput.*, vol. 43, no. 4, B884–B906, 2021.

[9] D. Chappell, M. Richter, G. Tanner, O. Bandtlow, W. Just, and J. Slipantschuk, "Ray-tracing the Ulam way", in *International Conference on Integral Methods in Science and Engineering*, Springer, 2022, pp. 95–101.

[10] J. Slipantschuk, M. Richter, D. J. Chappell, G. Tanner, W. Just, and O. F. Bandtlow, "Transfer operator approach to ray-tracing in circular domains", *Nonlinearity*, vol. 33, no. 11, p. 5773, 2020.

[11] M. Williams, I. Kevrekidis, and C. Rowley, "A data-driven approximation of the Koopman operator: Extending dynamic mode decomposition", *Journal of Nonlinear Science*, vol. 25, pp. 1307–1346, 2015.

[12] S. Klus, F. Nuske, P. Koltai, H. Wu, I. Kevrekidis, C. Shutte, and F. Noe, "Data-driven model reduction and transfer operator approximation", *Journal of Nonlinear Science*, vol. 28, pp. 985–1010, 2018.

[13] J. Bajars, D. Chappell, T. Hartmann, and G. Tanner, "Improved approximation of phase-space densities on triangulated domains using discrete flow mapping with p-refinement", *Journal of Scientific Computing*, vol. 72, pp. 1290–1312, 2017.